Review 1

Sb^{5+} and Sb^{3+} substitution in segnitite: a new sink for As and Sb in the environment and implications for acid mine drainage

Stuart J. Mills[1], Barbara Etschmann[2], Anthony R. Kampf[3], Glenn Poirier[4] & Matthew Newville[5]

[1]Geosciences, Museum Victoria, GPO Box 666, Melbourne 3001, Victoria, Australia

[2]Mineralogy, South Australian Museum, North Terrace, Adelaide 5000 Australia + School of Chemical Engineering, The University of Adelaide, North Terrace 5005, Australia

[3]Mineral Sciences Department, Natural History Museum of Los Angeles County, 900 Exposition Boulevard, Los Angeles, California 90007, U.S.A.

[4]Mineral Sciences Division, Canadian Museum of Nature, P.O. Box 3443, Station D, Ottawa, Ontario, Canada, K1P 6P4

[5]Center for Advanced Radiation Studies, University of Chicago, Building 434A, Argonne National Laboratory, Argonne. IL 60439, U.S.A.

*E-mail: smills@museum.vic.gov.au

Abstract

A sample of Sb-rich segnitite from the Black Pine mine, Montana, USA has been studied by microprobe analyses, single crystal X-ray diffraction, μ-EXAFS and XANES spectroscopy. Linear combination fitting of the spectroscopic data provided Sb^{5+}:Sb^{3+} = 85(2):15(2), where Sb^{5+} is in octahedral coordination substituting for Fe^{3+} and Sb^{3+} is in tetrahedral coordination substituting for As^{5+}. Based upon this Sb^{5+}:Sb^{3+} ratio, the microprobe analyses yielded the empirical formula $Pb_{1.02}H_{1.02}(Fe^{3+}_{2.36}Sb^{5+}_{0.41}Cu^{2+}_{0.27})_{\Sigma 3.04}(As^{5+}_{1.78}Sb^{3+}_{0.07}S^{6+}_{0.02})_{\Sigma 1.88}O_8(OH)_{6.00}$. The crystal structure refinement and bond valence analysis are consistent with these cation site assignments. The formation of Sb-rich segnitite opens new possibilities for Sb sinks within the supergene zone. Segnitite may, in fact, be an ideal host for the sequestering of a number of toxic elements for pH < 2. At higher pH values, As is more likely to be incorporated into schwertmannite and ferrihydrite.

Keywords: EXAFS, XANES, crystal structure, segnitite, antimony, valency, alunite supergroup, oxidized zone.

Introduction

Segnitite, ideally $PbFe^{3+}_3(AsO_4)_2(OH,H_2O)_6$ (Birch et al. 1992), is the Pb□Fe-rich member of the dussertite group, within the alunite supergroup (Mills et al. 2009a; Bayliss et al. 2010). It forms solid solution series with both kintoreite and beudantite (e.g. Rattray et al. 1996; Jambor 1999; Mills 2007), and it has been observed at more than 100 localities worldwide (www.mindat.org).

Minerals in the alunite supergroup have the general formula $AB_3(TO_4)_2X_6$, where the *A*-site can be occupied by monovalent (Na^+, K^+, Ag^+, NH_4^+ or H_3O^+), divalent (Pb^{2+}, Ca^{2+} or Ba^{2+}), or trivalent (Bi^{3+} or REE^{3+}) cations; the *B*-site can be occupied by either Fe^{3+}, Al^{3+}or Ga^{3+}, whilst the *T* cation site can be occupied by P^{5+}, S^{6+} or As^{5+} (e.g. Jambor, 1999). The supergroup has always been of significant interest to mineral scientists especially because of its relevance to acid mine drainage (e.g., Nordstrom et al. 2000; Welch et al. 2007, 2008, 2009) and the mobility of toxic elements (e.g., Kolitsch & Pring 2001) and because of its structural variability (e.g., Grey et al. 2008; Mills et al. 2008). To date, however, there has been only one reported example of Sb substitution within a member of the supergroup. Kolitsch et al. (1999) reported the structure of "antimonian" dussertite from the Clara mine, Germany, and attributed all of the Sb to Sb^{5+} substituting for Fe^{3+} within the octahedral site. The find of an unusual Sb-rich segnitite from the Black Pine mine, Montana, USA, has prompted further investigation by us into the valency and structural role of Sb within members of the alunite supergroup.

Experimental

Sample

The Sb-rich segnitite occurs at the Black Pine mine, 14.5 km NW of Philipsburg, Granite Co., Montana, USA (46°26'52"N, 113°21'56"W), and was discovered by Mr. John Dagenais of Vancouver, B.C., Canada. The mineral occurs as flattened, tabular or rhombohedral yellowish crystals up to about 100 μm across. Crystals are commonly intergrown to form botryoidal groups up to about 0.3 mm across and also form as coatings lining quartz vughs and on quartz crystals. Associated minerals are hidalgoite and tetrahedrite. The Black Pine mine is the type locality for philipsburgite (Peacor *et al.,* 1985), joëlbruggerite (Mills *et al*., 2009a) and auriacusite (Mills *et al*., 2010). The studied specimen has been deposited in the collections of Mineral Sciences Department, Natural History Museum of Los Angeles County, catalogue number 64096.

X-ray Absorption Spectroscopy

Sb K-edge (30491 eV) X-ray Absorption Near Edge Structure (XANES) and micro Extended X-ray absorption Fine Structure (μ-EXAFS) spectra were measured at beam line 13-ID-C (GSE-CARS) at the Advanced Photon Source (APS), at Argonne, USA. The APS is a 7 GeV ring and operates in top-up mode with a current of 102 mA. 13-ID-C is an undulator beam line with a Si(111) monochromator and an energy resolution ($\Delta E/E$) of 1.4×10^{-4} at 10 keV. A focused beam size of 5 μm^2 was used. A 16 element solid-state Ge detector was used for detecting fluorescence data.

XANES and EXAFS data were analyzed with the HORAE package (Ravel and Newville 2005), calculations being performed using FEFF version 9 (Rehr et al. 2010). Self-absorption effects were checked for the fluorescence data using the SABCOR (Booth and Bridges 2005) correction routine that is incorporated into ATHENA (part of the HORAE package) and were found to be negligible. The data used in the EXAFS fits ranged from k = 2.0 to 10.0 $Å^{-1}$. The

fitting was done in R-space in the range 1.0□4.0 Å, with a Hanning window and multiple $k^{1,2,3}$ weighting.

Chemical analysis

Quantitative wavelength-dispersive electron-microprobe analyses (6 points) were carried out with a JEOL733 electron microprobe at the Mineral Sciences Division, Canadian Museum of Nature. Operating conditions were 20 kV, with beam current of 20 nA and a 2 μm beam diameter. Raw intensity data were corrected using a PAP matrix correction (Pouchou and Pichoir 1984). No other elements were detected by energy dispersive spectroscopy. Sb^{3+} and Sb^{5+} were apportioned based on the EXAFS and XANES reported below. H_2O was calculated based on the site populations. The results, as well as the standards used, are shown in **Table 1**.

X-ray diffraction

The single-crystal X-ray diffraction data were obtained on a Rigaku R-Axis Rapid II curved imaging plate microdiffractometer utilizing monochromatized Mo*K*α radiation. The Rigaku CrystalClear software package was used for processing of the diffraction data, including the application of an empirical multi-scan absorption correction using ABSCOR (Higashi 2001). The structure was solved by direct methods using SHELXS-97 software (Sheldrick 2008), and SHELXL-97 (Sheldrick 2008) was used for the refinement of the structure. The occupancies of the Fe and As sites were constrained to match the ratios obtained from the chemical and spectroscopic analyses below. The final model, anisotropically refined, converged to R_1 = 0.0303 for all 114 observed reflections [F_o>4σF_o] and 0.0333 for all 125 unique reflections. Details concerning data collection and structure refinement are provided

in **Table 2**. Fractional coordinates and atom displacement parameters are provided in **Table 3**, selected interatomic distances in **Table 4** and bond valence sums (BVS) in **Table 5**.

Results

μ-EXAFS and XANES

Linear combination fitting of the XANES spectra using standards Sb_2O_3 and $KSb(OH)_6$ (Mitsunobu et al. 2008) resulted in a ratio of Sb^{5+}:Sb^{3+} 85(2):15(2) (χ^2_{red} = 0.15). The fraction of Sb^{5+}:Sb^{3+} was refined in the EXAFS data by fitting a linear combination of octahedrally coordinated Sb^{5+}□O and tetrahedrally coordinated Sb^{3+}□O (**Table 6**). To reduce the number of variables, the spectra for three grains were co-refined. The best fit resulted with 100% Sb^{5+}□O; however, it is possible to obtain a fit that is visually as good and with a χ^2_{red} that is not statistically significantly different (Kelly et al. 2008) by fitting 85% octahederally coodinated Sb^{5+}□O and 15% tetrahedrally coordinated Sb^{3+}□O (**Figure 1**). Attempts to fit more Sb^{3+}□O resulted in unreasonable fit parameters. It is important to note that the microprobe analyses do not support having only As in the tetrahedral site, and tetrahedral vacancies are not known to occur in the alunite supergroup. Thus, all lines of evidence provide strong support for 15% Sb^{3+}□O being present in these grains.

Microprobe analyses

Based on the results of the μ-EXAFS and XANES above, we can recast the Sb_2O_5 in the microprobe analyses as Sb_2O_5 + Sb_2O_3 in the proportion 85:15. In doing so, we obtain the empirical formula $Pb_{1.02}H_{1.02}(Fe^{3+}_{2.36}Sb^{5+}_{0.41}Cu^{2+}_{0.27})_{\Sigma 3.04}(As^{5+}_{1.78}Sb^{3+}_{0.07}S^{6+}_{0.02})_{\Sigma 1.88}O_8(OH)_{6.00}$. It is interesting to note that although Sb^{5+} + Cu^{2+} > 0.5 *apfu*, because of the difference in valence between Sb^{5+} and Cu^{2+}, this phase does not qualify as a new mineral under the rule of *valency-imposed*

double site occupancy (Hatert et al. 2008), similar to beavertite-(Cu) or beavertite-(Zn) (Bayliss et al. 2010; Sato et al. 2011). If Sb^{5+} were > 0.5 *apfu* (substituting for Fe^{3+}), this mineral would qualify as a new mineral species.

Crystal structure

Segnitite has a rhombohedral alunite-type structure (e.g. Blount, 1974), consisting of layers of corner-sharing $FeO_2(OH)_4$ octahedra and AsO_4 tetrahedra parallel to (0001) and stacked along **c**. Pb atoms are displaced from the origin, as in other Pb species of the supergroup (e.g. philipsbornite, Cooper and Hawthorne 2012; plumbogummite, Mills et al. 2009c; kintoreite, Kharisun et al. 1997; Grey et al. 2009), and are in 12-fold coordination. The $Fe(O,OH)_6$ octahedra each share corners with four neighbours to form a planar kagomé network with 3- and 6-fold rings, which can also be described as hexagonal tungsten bronze (HTB)-type layers. The O^{2-} anions of the $Fe(O,OH)_6$ octahedra in each 3-ring link to an arsenate, either above or below the plane of the Fe layer. Successive layers are interconnected via hydrogen bonds from H to arsenate O1 of an adjacent layer (Figure 2).

The average bond lengths for Sb-rich segnitite are <Fe□O> = 2.007 Å, <As□O> = 1.685 Å and <Pb□O> = 2.84 Å. The average bond lengths for <Fe□O> and <As□O> are indistinguishable from those reported by Kolitsch et al. (1999) for "antimonian" dussertite, 2.009 and 1.684 Å, respectively. It is not be surprising that they are the same, given that there are many substitutions occurring in the Fe and As sites within the minerals. In the case of Sb-rich segnitite, the incorporation of Sb^{5+} in the Fe site would be expected to slightly shorten the average Fe□O bond length; while, Cu^{2+} would be expected to elongate it. These competing effects effectively cancel each other out. The BVS analysis provides a formal valency for the site of 2.13 *v.u.*, with a site charge of 3.23+, which matches well with the

theoretical of 3.17+. The <As□O> is close to the general average for arsenate tetrahedra of ~1.683 Å (Shannon and Calvo, 1973), despite the fact that Sb^{3+} at the site should result in longer bonds (the range observed for Sb^{3+}□O bonds is 1.80□3.50 Å; Mills et al. 2009b). It may be that the small amount of S (the general average S□O in sulfates is 1.459; Hawthorne et al. 2000) counteracts the effect of the Sb^{3+}. It is also noteworthy that the BVS for Pb and O2 show overbonding, which is typical in the Pb-rich members of the alunite supergroup (Mills et al. 2009d).

Implications

It is interesting to note that there are only two known minerals containing both Sb^{3+} and Sb^{5+}: cervanite, α-Sb_2O_4, a very common secondary mineral known from over two hundred localities (www.mindat.org), and clinocervantite, β-Sb_2O_4, a very rare secondary mineral only known from two localities in Italy (Basso et al. 1999). "Stibiconite" and "bismutostibiconite" may be mixed valency; however, both are considered questionable species (Atencio et al. 2010), and there is no spectroscopic data available to suggest that both Sb^{3+} and Sb^{5+} are present in these phases.

Antimony is considered a toxic heavy metal, and because of this, many studies have been aimed at understanding its behaviour in the supergene zone (e.g. Filella et al. 2009 and references therein). In the supergene zone, Sb is often found as a weathering bi-product associated with the mining of Sb sulphides and sulphosalts, such as stibnite, berthierite and tetrahedrite. The presence of Sb is often also coupled with the presence of As, and this may lead to severe environmental problems (e.g. Casiot et al. 2007; Majzlan et al. 2011; Mok and Wai 1990). Leverett et al. (2012) recently showed that the minerals schafarzikite, $FeSb_2O_4$, and tripuhyite, $FeSbO_4$, act as important sinks for the element, while Majzlan et al. (2011)

showed that tripuhyite was the main sink for Sb in the mine drainage tailings near Pezinok, Slovakia, and that As was concentrated in amorphous oxide phases.

The formation of Sb-rich segnitite, therefore, opens new possibilities for Sb sinks within the supergene zone. The Sb-rich segnitite contains on average about 28.93 wt % PbO, 25.88 wt % As_2O_5, 6.33 wt % Sb_2O_5 and 2.44 wt % Sb_2O_3, showing that substantial amounts of toxic elements can be locked away within the crystal structure of the mineral. In the case of the neutral (pH range 6.5–8.0) tailings reported by Majzlan et al. (2011), it may be the case that the mining tailings were at too high a pH for the formation of crystalline samples and/or members of the alunite supergroup. Mills (2007) showed that segnitite could be synthesised by hydrothermal methods in the pH range 1.0–1.5, indicating that under more acidic conditions this could be a preferred sink for Pb, Fe, Sb and As. Acidic river waters with low pH, such as those observed at Rio Tinto in Spain (pH range 1.5□2.7), exhibit a number of jarosite group species (e.g. jarosite, natrojarosite and plumbojarosite) and show the potential for sequestering a large number of toxic elements (Hudson-Edwards et al. 1999). Welch et al. (2008) showed that jarosite dissolution is slow, making jarosite-group minerals good hosts for sequestering toxic elements as long as the prevailing fluids remain at high pH. Insofar as the precipitation of segnitite or other alunite-supergroup species, the main barrier appears to be competition with As incorporation into schwertmannite and ferrihydrite (e.g. Carlson et al. 2002), which precipitate at higher pH values, 2.8□4.5 for schwertmannite and > 6.5 for ferrihydrite (Bigham et al. 1996).

At the Black Pine mine, Mills et al. (2009c) deduced that joëlbruggerite, $Pb_3Zn_3(Sb^{5+},Te^{6+})As_2O_{13}(OH,O)$, formed in a highly oxidizing environment, in water in near equilibrium with atmospheric oxygen [log $a_{O2(aq)}$ = –3.58] and a pH < 3. While cervantite

appears to form over a wide stability range (Roper et al. 2012), Sb-rich segnitite appears to have formed in a much narrower range typified by highly oxidising conditions and pH < 2.

Acknowledgements

We thank Ritsuro Miyawaki, an anonymous reviewer and Associate Editor Diego Gatta who provided helpful comments on the manuscript. The GeoSoilEnviroCARS (GSECARS) beamline at the APS is supported by the National Science Foundation – Earth Sciences (EAR-0622171) and Department of Energy – Geosciences (DE-FG02-94ER14466). Part of this study was also was funded by the John Jago Trelawney Endowment to the Mineral Sciences Department of the Natural History Museum of Los Angeles County. Peter Williams is also thanked for his insight on the role of Sb in the environment.

References

Atencio, D., Andrade, M.B., Christy, A.G., Gieré, R., and Kartashov, P.M. (2010) The pyrochlore supergroup of minerals: nomenclature. Canadian Mineralogist, 48, 673□698.

Basso, R., Lucchetti, G., Zefiro, L., and Palenzona, A. (1999) Clinocervantite, β-Sb_2O_4, the natural monoclinic polymorph of cervantite from the Cetine Mine, Siena, Italy. European Journal of Mineralogy, 11, 95□100.

Bayliss, P., Kolitsch, U., Nickel, E.H., and Pring, A. (2010) Alunite supergroup: recommended nomenclature. Mineralogical Magazine, 74, 919□927.

Bigham, J.M., Schwertmann, U., Traina, S.J., Winland, R.L., and Wolf, M. (1996) Schwertmannite and the chemical modeling of iron in acid sulfate waters. Geochimica et Cosmochimica Acta, 60, 2111□2121.

Birch, W.D., Pring, A., and Gatehouse, B.M. (1992) Segnitite, $PbFe_3H(AsO_4)_2(OH)_6$, a new mineral in the lusungite group from Broken Hill, New South Wales, Australia. American Mineralogist, 77, 656□659.

Blount, A.M. (1974) The crystal structure of crandallite. American Mineralogist, 59, 41□47.

Booth, C.H., and Bridges, F. (2005) Improved self-absorption correction for fluorescence measurements of extended X-ray absorption fine-structure. Physica Scripta, T115, 202–204.

Brown, I.D., and Altermatt, D. (1985) Bond-valence parameters from a systematic analysis of the inorganic crystal structure database. Acta Crystallographica, B41, 244–247.

Carlson, L., Bigham, J.M., Schwertmann, U., Kyek, A., and Wagner, F. (2002) Scavenging of As from acid mine drainage by schwertmannite and ferrihydrite: a comparison with synthetic analogues. Environmental Science & Technology, 36, 1712□1719.

Casiot, C., Ujevic, M., Munoz, M., Seidel, J. L., and Elbaz-Poulichet, F. (2007) Antimony and arsenic mobility in a creek draining an antimony mine abandoned 85 years ago (upper Orb basin, France). Applied Geochemistry, 22, 788□798.

Cooper, M.A., and Hawthorne, F.C. (2012) Refinement of the crystal structure of zoned philipsbornite–hidalgoite from the Tsumeb mine, Namibia, and hydrogen bonding in the $D^{2+}(T^{5+}O_4)(TO_3OH)(OH)_6$ alunite structures. Mineralogical Magazine, 76, 839□849.

Filella, M., Williams, P. A., and Belzile, N. (2009) Antimony in the environment: knowns and unknowns. Environmental Chemistry, 6, 95□105.

Grey, I.E., Mumme, W.G., Bordet, P., and Mills, S.J. (2008) A new crystal-chemical variation of the alunite-type structure in monoclinic $PbZn_{0.5}Fe_3(AsO_4)_2(OH)_6$. Canadian Mineralogist, 46, 1355□1364.

Grey, I.E., Mumme, W.G., Mills, S.J., Birch, W.D., and Wilson, N.C. (2009) The crystal chemical role of Zn in alunite-type minerals: structure refinements for kintoreite and zincian kintoreite. American Mineralogist, 94, 676□683.

Hatert, F., and Burke, E.A. (2008) The IMA–CNMNC dominant-constituent rule revisited and extended. Canadian Mineralogist, 46, 717□728.

Hawthorne, F. C., Krivovichev, S. V., and Burns, P. C. (2000) The crystal chemistry of sulfate minerals. Reviews in Mineralogy and Geochemistry, 40, 1□112.

Higashi, T. (2001) ABSCOR. Rigaku Corporation, Tokyo, Japan.

Hudson-Edwards, K.A., Schell, C., and Macklin, M.G. (1999) Mineralogy and geochemistry of alluvium contaminated by metal mining in the Rio Tinto area, southwest Spain. Applied Geochemistry, 14, 1015□1030.

Jambor, J.L. (1999) Nomenclature of the alunite supergroup. Canadian Mineralogist, 37, 1323□1341.

Kelly, S., Hesterberg, D., and Ravel, B. (2008) Analysis of soils and minerals using X-ray absorption spectroscopy. In: *Methods of Soil Analysis, Part 5. Mineralogical Methods*. Soil Sciences Society of America, Madison, USA, 387–463.

Kharisun, Taylor, M.R., Bevan, D.J.M., and Pring, A. (1997) The crystal structure of kintoreite, $PbFe_3(PO_4)_2(OH,H_2O)_6$. Mineralogical Magazine, 61, 123□129.

Kolitsch, U., and Pring, A. (2001) Crystal chemistry of the crandallite, beudantite and alunite groups: a review and evaluation of the suitability as storage materials for toxic metals. Journal of Mineralogical and Petrological Sciences, 96, 67–78.

Kolitsch, U., Slade, P.G., Tiekink, E.R.T., and Pring, A. (1999) The structure of antimonian dussertite and the role of antimony in oxysalt minerals. Mineralogical Magazine, 63, 17–26.

Krivovichev, S. V., and Brown, I. D. (2001) Are the compressive effects of encapsulation an artifact of the bond valence parameters? Zeitschrift für Kristallographie, 216, 245–247.

Leverett, P., Reynolds, J.K., Roper, A.J., and Williams, P.A. (2012) Tripuhyite and schafarzikite: two of the ultimate sinks for antimony in the natural environment. Mineralogical Magazine, 76, 891–902.

Majzlan, J., Lalinská, B., Chovan, M., Bläß, U., Brecht, B., Göttlicher, J., Steininger, R., Hug, K., Ziegler, S., and Gescher, J. (2011) A mineralogical, geochemical, and microbiogical assessment of the antimony-and arsenic-rich neutral mine drainage tailings near Pezinok, Slovakia. American Mineralogist, 96, 1–13.

Mills, S.J. (2007) *The crystal chemistry and geochronology of minerals from Broken Hill*. Unpublished PhD Thesis, School of Earth Sciences, University of Melbourne.

Mills, S.J., Christy, A.G., Chen, E.C.C., and Raudsepp, M. (2009b) Revised values of the bond valence parameters for $^{[6]}$Sb(V)-O and $^{[3\text{-}11]}$Sb(III)-O. Zeitschrift für Kristallographie, 224, 423–431.

Mills, S.J., Grey, I.E., Mumme, W.G., Miyawaki, R., Matsubara, S., Bordet, P., Birch, W.D., and Raudsepp, M. (2008) Kolitschite, $Pb[Zn_{0.5},\square_{0.5}]Fe_3(AsO_4)_2(OH)_6$, a new mineral from the Kintore opencut, Broken Hill. Australian Journal of Mineralogy, 14, 63–67.

Mills, S.J., Hatert, F., Nickel, E.H., and Ferraris, G. (2009a) The standardisation of mineral group hierarchies: application to recent nomenclature proposals. European Journal of Mineralogy, 21, 1073–1080.

Mills, S.J., Kampf, A.R., Poirier, G., Raudsepp, M., and Steel, I.M. (2010) Auriacusite, $Fe^{3+}Cu^{2+}(As,Sb)O_4O$, the first M^{3+} member of the olivenite group, from the Black Pine mine, Montana, USA. Mineralogy and Petrology, 99, 113–120.

Mills, S.J., Kampf, A.R., Raudsepp, M., and Christy, A.G. (2009d) The crystal structure of Ga-rich plumbogummite from Tsumeb, Namibia. Mineralogical Magazine, 73, 837–845.

Mills, S.J., Kolitsch, U., Miyawaki, R., Groat, L.A., and Poirier, G. (2009c) Joëlbruggerite, $Pb_3Zn_3(Sb^{5+},Te^{6+})As_2O_{13}(OH,O)$, the Sb^{5+} analogue of dugganite, from the Black Pine mine. Montana. American Mineralogist, 94, 1012–1017.

Mitsunobu, S., Takahashi, Y., Sakai, Y., and Inumaru, K. (2008) Interaction of synthetic sulfate green rust with antimony (V). Environmental Science & Technology, 43, 318–323.

Mok, W.M. and Wai, C.M. (1990) Distribution and mobilization of arsenic and antimony species in the Coeur d'Alene River, Idaho. Environmental Science & Technology, 24, 102□108.

Nordstrom, D.K., Alpers, C.N., Ptacek, C.J., and Blowes D.W. (2000) Negative pH and extremely acidic mine waters from Iron Mountain, California. Environmental Science & Technology, 34, 254□258.

Peacor, D.R., Dunn, P.J., Ramik, R.A., Sturman, B.D., and Zeihan, L.G. (1985) Philipsburgite, a new copper zinc arsenate hydrate related to kipushite, from Montana. Canadian Mineralogist, 23, 255–258.

Pouchou, J. L., and Pichoir, F. (1984) A New Model for Quantitative X-Ray Microanalysis. I. Application to the Analysis of Homogeneous Samples. Rech Aerospatiale, 3, 167□192.

Rattray, K.J., Taylor, M.R., Bevan, D.J.M., and Pring, A. (1996) Compositional segregation and solid solution in the lead-dominant alunite-type minerals from Broken Hill, NSW. Mineralogical Magazine, 60, 779□786.

Ravel, B., and Newville, M. (2005) ATHENA, ARTEMIS, HEPHAESTUS: data analysis for X-ray absorption spectroscopy using IFEFFIT. Journal of Synchrotron Radiatation, 12, 537–541.

Rehr, J.J., Kas, J.J., Vila, F.D., Prange, M.P., and Jorissen, K. (2010) Parameter-free calculations of X-ray spectra with FEFF9. Physical Chemistry Chemical Physics, 12, 5503–5513.

Roper, A.J., Williams, P.A., and Filella, M. (2012) Secondary antimony minerals: phases that control the dispersion of antimony in the supergene zone. Chemie der Erde-Geochemistry, 72, 9□14.

Sato, E., Nakai, I., Terada, Y., Tsutsumi, Y., Yokoyama, K., Miyawaki, R., and Matsubara, S. (2011) Beaverite-(Zn), $Pb(Fe_2Zn)(SO4)_2(OH)$, a new member of the alunite group, from Mikawa Mine, Niigata Prefecture, Japan. Mineralogical Magazine, 75, 375□377.

Shannon, R.T., and Calvo, C. (1973) Refinement of the crystal structure of low temperature Li_3VO_4 and analysis of mean bond lengths in phosphates, arsenates, and vanadates. Journal of Solid State Chemistry, 6, 538□549.

Sheldrick, G.M. (2008) A short history of SHELX. Acta Crystallographica, A64, 112□122.

Welch, S.A., Christy, A.G., Kirste, D., Beavis, S.G., and Beavis, F. (2007) Jarosite dissolution I – trace cation flux in acid sulfate soils. Chemical Geology, 245, 183□197.

Welch, S.A., Kirste, D., Christy, A.G., Beavis, F.R., and Beavis, S.G. (2008) Jarosite dissolution II – reaction kinetics, stoichiometry and acid flux. Chemical Geology, 254, 73□86.

Welch, S.A., Christy, A.G., Isaacson, L., and Kirste, D. (2009) Mineralogical control of rare earth elements in acid sulfate soils. Geochimica et Cosmochimica Acta, 73, 44□64.

Table 1. Chemical analytical data for the Sb-rich segnitite.

	average	min	max	standards
PbO	28.84	28.17	29.48	galena
CuO	2.73	2.59	2.84	cuprite
Fe_2O_3	23.86	23.01	25.34	hematite
*Sb_2O_5**	*9.85*	*7.86*	*11.19*	*Sb_2Te*
Sb_2O_5*	8.37	6.68	9.51	
Sb_2O_3*	1.33	1.06	1.51	
As_2O_5	25.92	25.54	26.26	GaAs
SO_3	0.25	0.16	0.30	pentlandite
H_2O_{calc}	8.01			
Total	99.31			

*recast into Sb_2O_5 and Sb_2O_3 based on 85:15 ratio.

Table 2. Data collection and structure refinement details for the Sb-rich segnitite.

Space group	*R*-3*m*
Unit cell dimensions	
a (Å)	7.3730(14)
c (Å)	17.228(3)
V (Å^3)	811.0(3)
Z	3
Absorption coefficient	26.452
F(000)	1073
° range	3.40□20.80
Index ranges	$-7 \le h \le 7, -7 \le k \le 7, -16 \le l \le 17$
Reflections collected/unique	1342 / 125
Reflections with $F > 4\sigma(F)$	114
Refinement method	Full-matrix least-squares on F^2
Parameters refined	31
GoF	1.22
Final *R* indices [$F_o > 4\sigma(F)$]	0.0303
R indices (all data)	0.0333
Extinction coefficient	0.0006(3)
Largest diff. peak / hole	+0.58, -0.81 e A^{-3}

416 Table 3. Fractional coordinates and atomic displacement parameters for the Sb-rich segnitite.
417

	x	*y*	*z*	U_{eq}	*occy.*	U_{11}	U_{22}	U_{33}	U_{23}	U_{13}	U_{12}
Pb	0.044(11)	0	0	0.032(17)	1	0.030(14)	0.03(5)	0.0357(17)	-0.006(8)	-0.003(4)	0.01(3)
Fe1	0.5	0	0.5	0.0097(11)	0.78	0.0088(15)	0.0070(18)	0.0129(18)	0.0023(13)	0.0012(6)	0.0035(9)
Sb1	0.5	0	0.5	0.0097(11)	0.13	0.0088(15)	0.0070(18)	0.0129(18)	0.0023(13)	0.0012(6)	0.0035(9)
Cu1	0.5	0	0.5	0.0097(11)	0.09	0.0088(15)	0.0070(18)	0.0129(18)	0.0023(13)	0.0012(6)	0.0035(9)
As2	0	0	0.31346(18)	0.0194(12)	0.95	0.0180(14)	0.0180(14)	0.022(2)	0	0	0.0090(7)
Sb2	0	0	0.31346(18)	0.0194(12)	0.04	0.0180(14)	0.0180(14)	0.022(2)	0	0	0.0090(7)
S2	0	0	0.31346(18)	0.0194(12)	0.02	0.0180(14)	0.0180(14)	0.022(2)	0	0	0.0090(7)
O1	0	0	0.5890(12)	0.030(6)	1	0.038(9)	0.038(9)	0.014(12)	0	0	0.019(4)
O2	0.2093(8)	-0.2093(8)	-0.0536(7)	0.019(3)	1	0.019(5)	0.019(5)	0.024(7)	0.001(3)	-0.001(3)	0.013(6)
O3	0.1261(8)	-0.1261(8)	0.1349(6)	0.017(3)	1	0.009(5)	0.009(5)	0.034(8)	-0.004(3)	0.004(3)	0.007(5)
H1	0.196(2)	-0.196(2)	0.129(9)	0.02	1						

418 Table 4. Selected bond lengths (Å) in the Sb-rich segnitite.
419

Fe1	O3	1.999(4)	×4
	O2	2.022(11)	×2
<Fe1□O>		2.007	
As2	O1	1.68(2)	
	O2	1.687(11)	×3
<As2□O>		1.685	
Pb	O2	2.57(7)	×2
	O3	2.68(4)	×2
	O3	2.84(4)	×2
	O2	2.85(4)	×2
	O3	3.00(4)	×2
	O2	3.10(4)	×2
<Pb□O>		2.84	

420

421

422 Table 5. Bond valence sums for the Sb-rich segnitite. Values are expressed in valence units.
423

	Pb		Fe		As		H	Σ
O1					1.29		0.3	1.59
O2	0.55	↓×2	0.52	↓×2	1.24	↓×3		2.31
O3	0.52	↓×2	0.55	↓×4			0.7	2.03
Σ	2.14		2.13		5.00			

424 *Notes*: Pb–O bond strengths from Krivovichev and Brown (2001); Sb–O from Mills et al. (2009b);
425 Fe–O, Cu–O, As–O and H–O bond strengths from Brown and Altermatt (1985).
426

427

428

429

430

431

Table 6. EXAFS refinement parameters.

Sample	Fit	Site	Ligand	R (Å)	σ^2 (Å^2)	ΔE_0 (eV)	χ^2_{red}
Grain2	**1**. 100% Sb^{5+}	Oct	Sb^{5+}□O_6	1.965(7)	0.0027(5)	5.9(8)	103.5
		Oct	Multiple scattering paths	3.365(7) 3.930(7)	0.0027(5)		
Grain3	**1**. 100% Sb^{5+}	Oct	Sb^{5+}□O_6	1.969(8)	0.0027(5)	5.9(8)	103.5
		Oct	Multiple scattering paths	3.370(8) 3.937(8)	0.0027(5)		
Grain1	**1**. 100% Sb^{5+}	Oct	Sb^{5+}□O_6	1.96(1)	0.0027(5)	5.9(8)	103.5
		Oct	Multiple scattering paths	3.36(1) 3.93(1)	0.0027(5)		
Grain2	**2**. 85% Sb^{5+} + 15% Sb^{3+}	Oct	Sb^{5+}□O_6	1.963(7)	0.0004(5)	4.9(7)	114.5
		Oct	Multiple scattering paths	3.361(7) 3.925(7)			
		Tet	Sb^{3+}□O_4	1.80 (fix)			
Grain3	**2**. 85% Sb^{5+} + 15% Sb^{3+}	Oct	Sb^{5+}□O_6	1.965(8)	0.0004(5)	4.9(7)	114.5
		Oct	Multiple scattering paths	3.365(8) 3.931(8)			
		Tet	Sb^{3+}□O_4	1.80 (fix)			
Grain1	**2**. 85% Sb^{5+} + 15% Sb^{3+}	Oct	Sb^{5+}□O_6	1.96(1)	0.0004(5)	4.9(7)	114.5
		Oct	Multiple scattering paths	3.36(1) 3.92(1)			
		Tet	Sb^{3+}□O_4	1.80 (fix)			

442 Figure 1. Sb K-edge EXAFS fits for three Sb-rich segnitite grains.

443

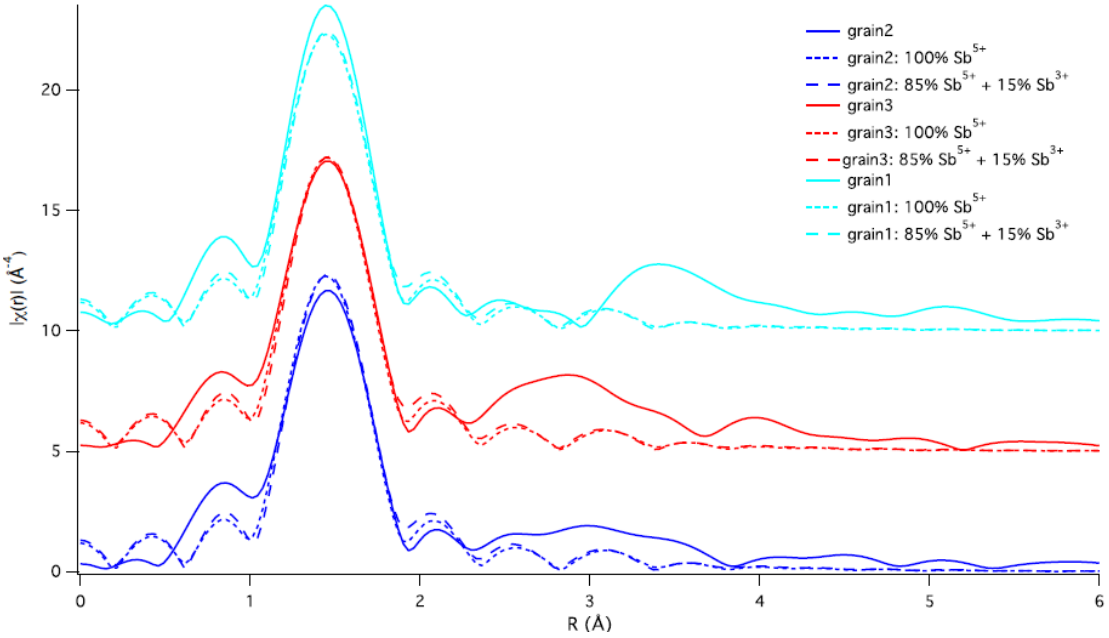

444

445

446

447

448

449

450

451

452

453

454

455

456

457

458

459 Figure 2. The crystal structure of Sb-rich segnitite viewed down [110]. FeO_6 octahedra are
460 orange, AsO_4 tetrahedra green, Pb atoms are grey and H atoms pink.

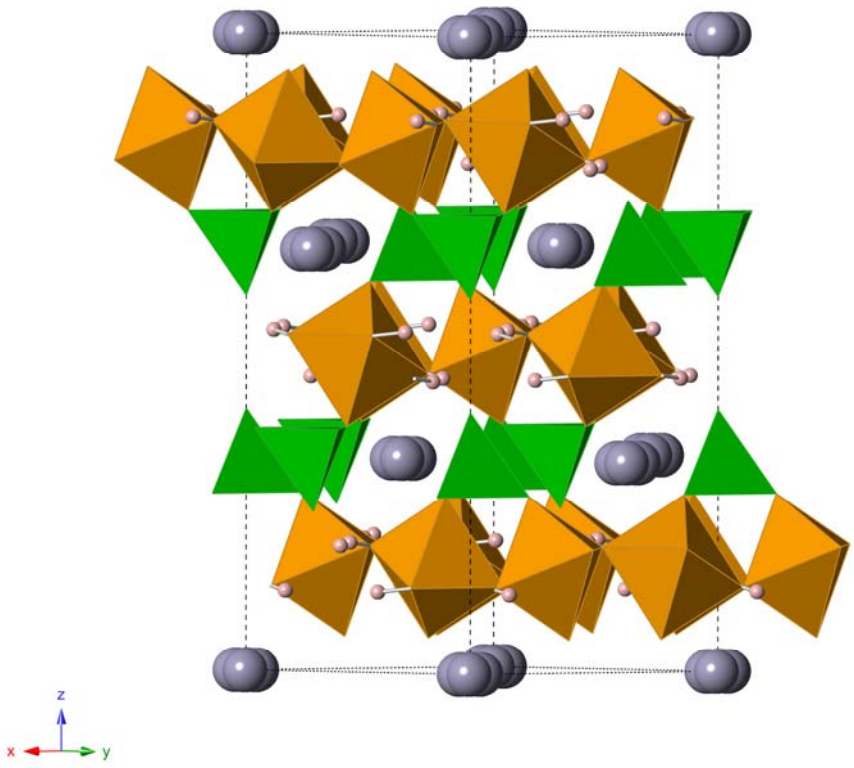

461

This is a preprint, the final version is subject to change, of the American Mineralogist (MSA)
Cite as Authors (Year) Title. American Mineralogist, in press.
(DOI will not work until issue is live.) DOI: http://dx.doi.org/10.2138/am.2014.4834

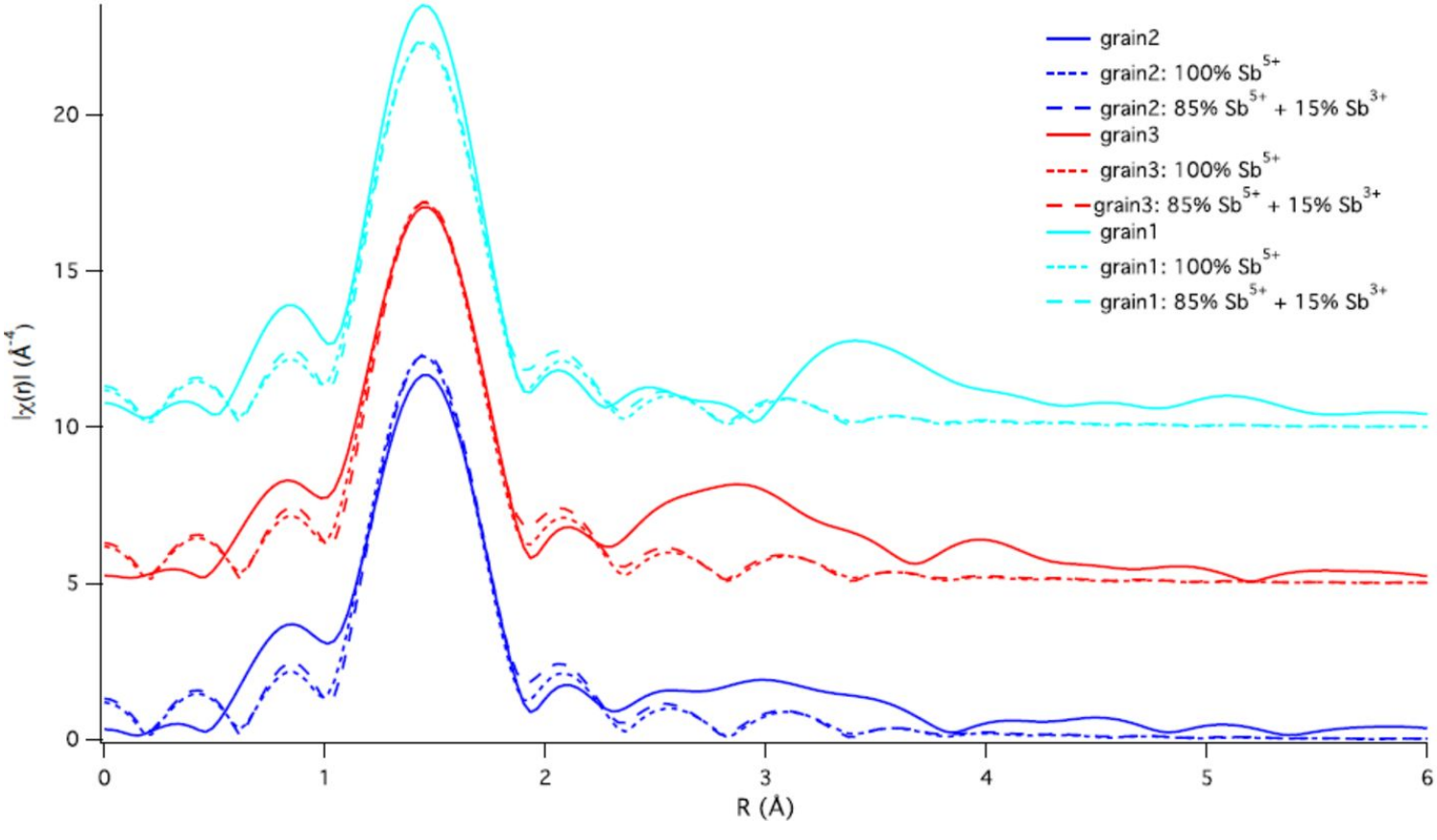

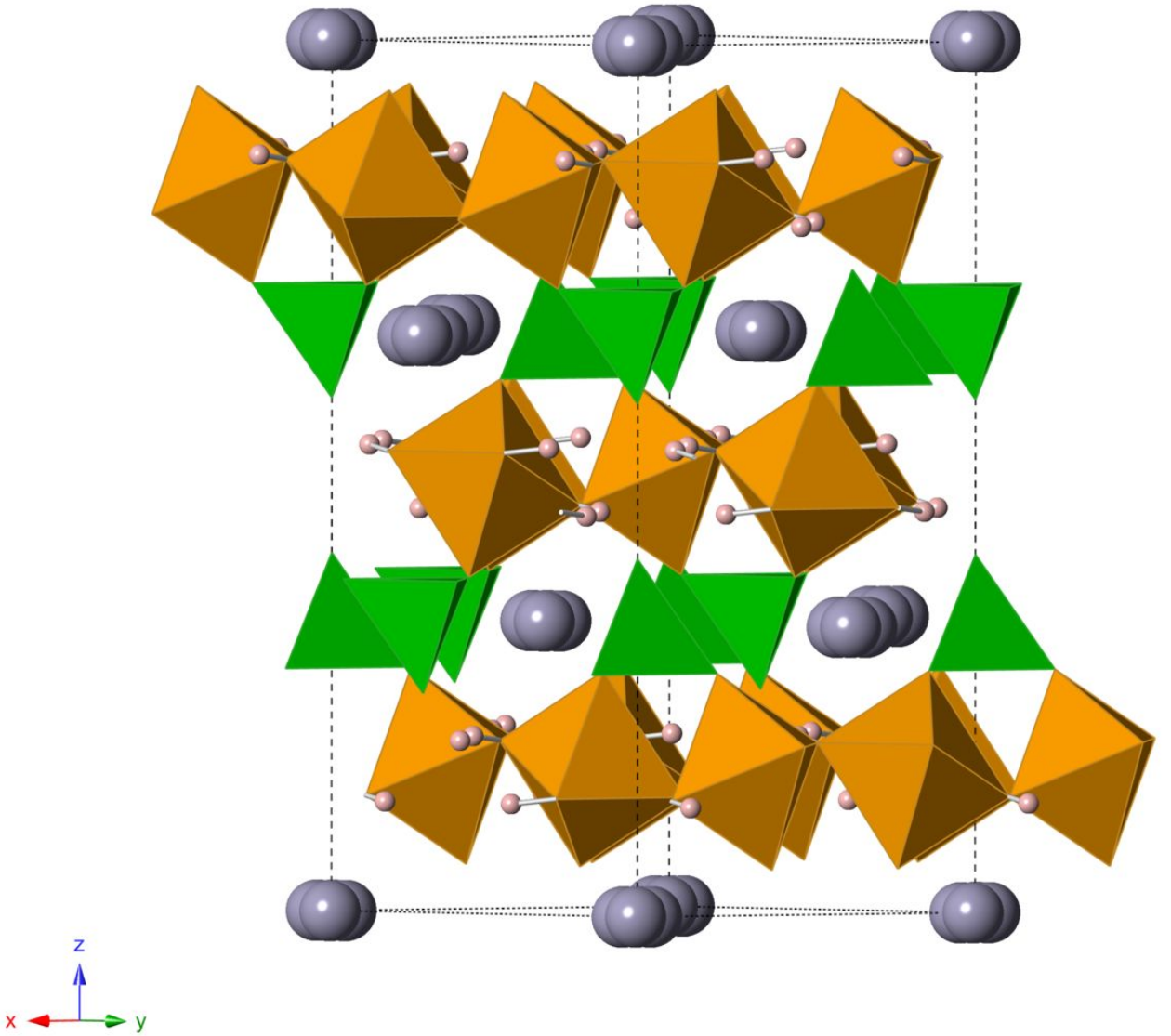
z
x
y